Drag law for an intruder in granular sediments

Andreea Panaitescu, Xavier Clotet, and Arshad Kudrolli*
Department of Physics, Clark University, Worcester, Massachusetts 01610, USA
(Received 29 October 2016; published 2 March 2017)

We investigate the drag experienced by a spherical intruder moving through a medium consisting of granular hydrogels immersed in water as a function of its depth, size, and speed. The medium is observed to display a yield stress with a finite force required to move the intruder in the quasistatic regime at low speeds before rapidly increasing at high speeds. In order to understand the relevant time scales that determine drag, we estimate the inertial number I given by the ratio of the time scales required to rearrange grains due to the overburden pressure and imposed shear and the viscous number J given by the ratio of the time scales required to sediment grains in the interstitial fluid and imposed shear. We find that the effective friction μ_e encountered by the intruder can be parametrized by $I = \sqrt{\rho_g/P_p}v_i$, where ρ_g is the density of the granular hydrogels, v_i is the intruder speed, and P_p is the overburden pressure due to the weight of the medium, over a wide range of I where the Stokes number $\mathrm{St} = I^2/J \gg 1$. We then show that μ_e can be described by the function $\mu_e(I) = \mu_0 + \alpha I^\beta$, where μ_0, α, and β are constants that depend on the medium. This formula can be used to predict the drag experienced by an intruder of a different size at a different depth in the same medium as a function of its speed.

DOI: 10.1103/PhysRevE.95.032901

I. INTRODUCTION

Objects moving through a viscoplastic medium composed of granular materials sedimented in a liquid are encountered widely at the bottom of water bodies and in the processing of petroleum and consumer products [1]. While a number of studies have investigated the force acting on an object moving through noncohesive granular matter in air [2–6] and in liquids [7], a robust friction law for the drag encountered by the intruder is not available. In the case of a granular medium immersed in a liquid where grains are always in contact, friction encountered has been found to be unchanged from the dry case [8]. Above this quasistatic limit, the intruder motion leads to inhomogeneous fluidization of the medium, giving rise to challenging problems in modeling their dynamics [9,10]. Because sedimented grains are densely packed and in contact, the granular stress can be expected to increase with depth, leading to sensitive variation in the dissipation encountered by an intruder as a function of depth. Furthermore, the relative importance of the granular and fluid components of the medium on the drag experienced by the intruder in this context remains undetermined.

Rheological properties of viscoplastic media are typically fitted to the Herschel-Bulkley model and its variations that relate the stress applied to the medium to the resulting strain rate of the medium [11,12]. Further, progress has been made recently [13–15] in describing the effective friction experienced by granular materials sheared uniformly under steady-state conditions using the inertial number I. This parameter, which is proportional to the strain rate, characterizes the ratio of the time scale over which grains rearrange due to pressure and the time scale required for grains to move past each other due to applied shear. In the case of neutrally buoyant non-Brownian suspensions immersed in a fluid, a constitutive law has been also proposed as a function of the viscous number J that characterizes the ratio of the time scale over which grains sediment and the time scale over which they rearrange due to applied pressure under steady-state conditions [16]. Further numerical simulations appear to suggest that the effective friction encountered by a uniformly sheared granular medium immersed in a fluid can be described by a combination of I and J, as $K = \gamma I^2 + J$, where γ is a constant that depends on the relative importance of inertia and viscosity of the medium [17]. However, it remains unclear how these descriptions can be extended to transient systems and ones in which the solids have a higher mass density compared to the liquid as in the case of sedimented solids.

Here we probe the dynamics of an intruder moving through sedimented granular hydrogels immersed in water as a function of the properties of the intruder and the medium. We use this medium as a model because it enables a subtle examination of inertia, gravity, and viscosity on the intruder dynamics. We focus our study on the condition where the intruder is pulled with a constant speed. However, it should be noted that the resulting intruder motion still leads to unsteady flow of the medium as it is fluidized and accelerated around the intruder. We obtain the inertial number I and the viscous number J to understand the relative importance of grain inertia and fluid viscosity on the observed dynamics. By measuring drag, we find that the effective friction μ_e given by the ratio of the stress acting on the intruder and the overburden pressure can be parametrized by I over the range of experimental parameters investigated. We further discuss the overall form of the observed μ_e as a function of I, which can be used to relate the drag experienced at a particular depth and speed to an intruder with a different size moving with different speed and depth.

II. EXPERIMENTAL SYSTEM

A schematic of the experimental apparatus is shown in Fig. 1(a). A large rectangular tank with length $L = 91$ cm, width $W = 45$ cm, and height $H = 42.5$ cm is filled with granular hydrogels immersed in water in a temperature-controlled room maintained at $24.0 \pm 0.5\,^\circ$C. The tank size was chosen to

*akudrolli@clarku.edu

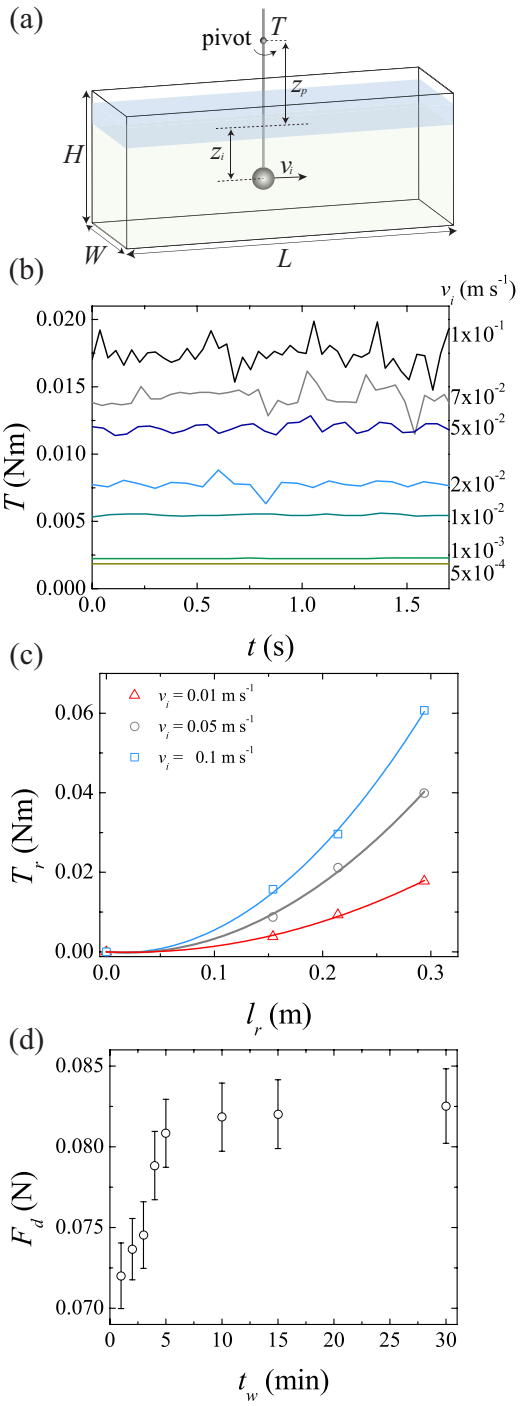

FIG. 1. (a) Schematic of the apparatus used to measure drag as a function of the intruder speed v_i and depth z_i. (b) Measured torque T as a function of time t for various v_i ($z_i = 20$ cm and $r_h = 0.5$ mm). (c) Torque T_r acting on the attachment rod as a function of immersion depth l_i with corresponding quadratic fits. The error bars in the measurements are less than the size of the markers and therefore are not drawn. (d) Measured drag F_d as a function of wait time t_w after the medium is stirred and allowed to settle.

be large enough that its boundaries do not affect the drag and thus the system can be considered as semi-infinite with only the distance to the bed surface playing a role in the measurements discussed in this study. The granular hydrogels were prepared by immersing dehydrated polyacrylamide particles in distilled water. Two sets of granular hydrogels with hydrated radius $r_h = 0.5 \pm 0.3$ and 8.5 ± 0.5 mm and density $\rho_h = 1004$ and 1006 kg m^{-3}, respectively, were used in the study. Because the grains are athermal and heavier than water (density $\rho_w = 998$ kg m^{-3} at 24 °C), they sediment to the bottom. A layer of clear water on the top prevents capillary effects from playing any role in the medium. The depth of this clear layer is not observed to have any measurable effect on the properties of the granular hydrogel medium below.

The volume fraction ϕ occupied by the sedimented granular hydrogels is estimated by measuring the volume of water displaced by the hydrogels. In the case of the smaller hydrogels, which are more polydisperse, we find $\phi \approx 0.5$, and in the case of the larger hydrogels, which are more monodisperse, $\phi \approx 0.6$, similar to sedimented frictional glass beads with similar size distribution [18]. Then the overburden pressure P_p at depth z due to the difference of density of the granular hydrogels and the water is given by $P_p = \phi(\rho_h - \rho_w)gz$, where g is the acceleration due to gravity. Although the granular hydrogels are relatively soft with a Young modulus E, which is measured [19] to be ≈23 kPa, the fractional change in their volume can be estimated from P_p/E to be less than 0.1% at the deepest point in the tank. Thus, we assume that the density of the medium $\rho_m = \phi\rho_h + (1-\phi)\rho_w$ is essentially constant for the purpose of our study. Substituting the values for ρ_h, ρ_w and ϕ, we obtain $\rho_m = 1001$ and 1003 kg m^{-3} for the small and large granular hydrogels, respectively.

In order to further quantify the effect of grain elasticity, we evaluate both the time scale due to elasticity T_k and the time scale due to gravity T_g [20]. We estimate T_k from the grain contact time scale $T_k = \sqrt{m/k_n}$, where m is the grain mass and $k_n \approx 2Er_h$ is the grain stiffness assuming linear contact. We then estimate T_g from the time taken by a grain to fall from rest through a distance r_h, i.e., $T_g = \sqrt{\frac{2r_h}{(1-\rho_w/\rho_h)g}}$. We obtain $T_k/T_g \approx 1.5 \times 10^{-2}$ and 0.4×10^{-2} in the case of the small and large hydrogels used in our study. The friction coefficient has been found to be relatively constant in numerical simulations for such contact times, relative to the time scale set by gravity [20].

A spherical intruder with a density similar to the hydrogels and radius r_i is fixed to the end of a stiff thin rod with radius r_r and immersed in the medium to a depth z_i as shown in Fig. 1(a). The rod is attached to a torque sensor and is translated along the length of the tank with speed v_i. The measurements are performed in the central third of the tank to avoid any effects of the tank walls. Because the medium is semitransparent because the hydrogels have a refractive index that is close to the water, we can observe the motion of the intruder and the medium around it. A movie of the motion of the medium obtained using a laser sheet as the intruder advances through the medium is shown in the Supplemental Material [21]. One observes that the grains accelerate around the intruder and quickly come to rest after the intruder passes by, similar to what one may expect in a viscous liquid. However, because the motion of the grains was difficult to track using automated algorithms, we were unable to extract quantitative information from the imaging. Hence, we focus on the measurement of drag experienced by the intruder using the torque sensor attached to the intruder in this study.

The torque T measured as function of time t is plotted in Fig. 1(b) and is observed to fluctuate around a constant value for a prescribed value of speed v_i. The mean torque $\langle T(t)\rangle$ is then obtained by averaging over time. The torque acting at the pivot has contributions because of the drag due to the intruder as well as the rod that attaches to the intruder in the medium. Therefore, we perform complementary measurements to account for the drag contribution due to the rod. The measured torque T_r as a function of the rod length immersed in the medium l_r is plotted in Fig. 1(c) at various speeds in the case of $d_h = 0.5$ mm and can be fitted as shown with a quadratic dependence on l_r. This quadratic form of drag with an increase of the depth of the rod has been found previously in the case of a dry granular medium in the quasistatic limit [22] and can be understood as follows. If the drag increases linearly with depth, then $T_r = F_d^r(z_p + \frac{2}{3}l_r)$, where z_p is the distance from the pivot to the medium surface as shown in Fig. 1(a). Indeed, as shown by the fit, we find that the torque increases quadratically with l_r, consistent with a linear increase of drag for a section of the rod with depth. This torque contribution is thus subtracted from the total mean torque to extract an approximate estimate of the torque T_i due to the intruder alone. Then we determine the drag acting on the intruder as $F_d = T_i/(z_p + l_r)$.

Further, we find that a systematic protocol has to be used while preparing the medium in order to obtain consistent data. In particular, drag measurements were conducted after stirring the medium, then allowing it to settle, and then waiting a fixed amount of time before pulling the intruder through the medium. Figure 1(d) shows the evolution of the measured drag F_d as a function of wait time t_w after the medium is stirred. One observes a significant variation over the first few minutes after the sediments are allowed to settle. The behavior stabilizes after approximately 10 min. Therefore, we use a wait time of 15 min before doing the systematic drag measurements as a function of system parameters reported in this study.

III. MEASUREMENT OF DRAG

The drag F_d measured as a function of the intruder speed v_i is plotted in Fig. 2(a) in the case of the media composed of the small and the large granular hydrogels but otherwise similar conditions. The data are plotted in a log-linear format to emphasize the wide range of intruder velocities probed. In each case, one observes that F_d appears essentially constant and well above zero at low v_i and increases rapidly as the velocity increases above $v_i \sim 1$ mm s^{-1}. Further, one observes that F_d is higher in the case of the larger grains compared with the smaller grains at low v_i, before crossing over as v_i is increased. Thus, the relative drag experienced by an intruder appears to depend on not only the medium, as one may expect, but also its speed.

To understand the measured drag in relation to the drag corresponding to the Newtonian fluid in which the grains are immersed, we obtain the estimate using $F_d^w = \frac{\pi}{2}C_d v_i^2 r_i^2$, where C_d is the drag coefficient of sphere. Then, using the approximation [23,24] $C_d \approx 24/\mathrm{Re}(1 + 0.15\,\mathrm{Re}^{0.687})$, where Re is the Reynolds number given by $\mathrm{Re} = \rho_w v_i r_i/\eta$, with the dynamic viscosity of water $\eta = 0.91$ mPa s, we calculate F_d^w and plot it in Fig. 2(a) over the same range of velocity. It is noted to be considerably smaller than the measured drag in the granular medium. Thus, although the hydrogel sediments have

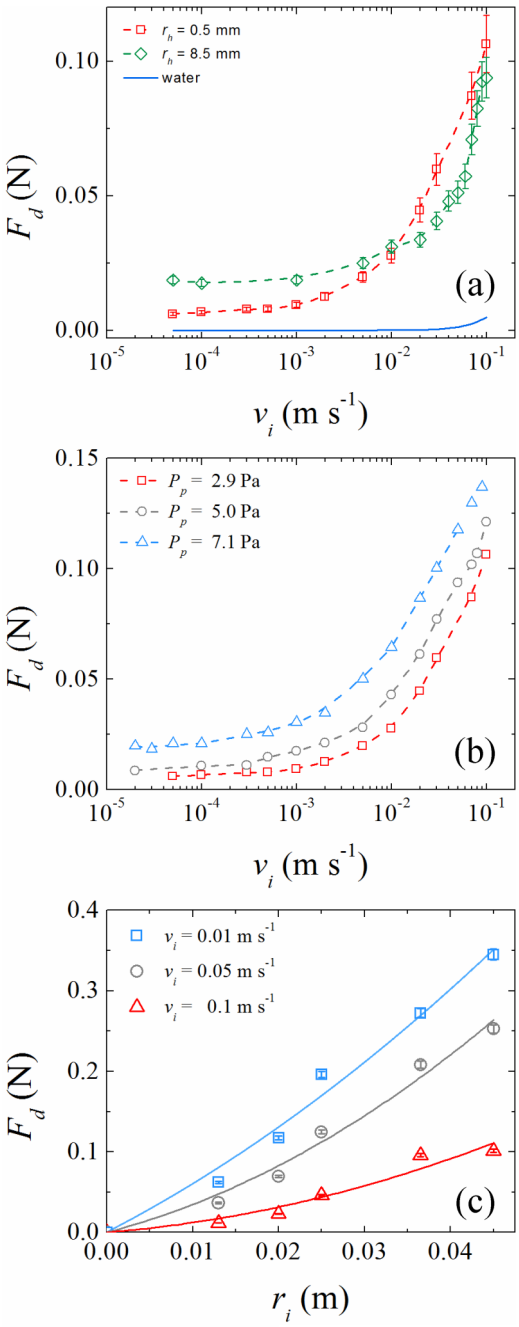

FIG. 2. (a) Measured drag F_d for an intruder as a function of v_i in the medium composed of the two different sized grains investigated in our experiments, but otherwise similar conditions. The error bars correspond to the standard deviation. The estimated drag in water for the same intruder size is also plotted for reference and is observed to be significantly lower than for the granular hydrogel medium. (b) Drag as a function of intruder speed v_i for various overburden pressures P_p corresponding to various depths ($r_h = 0.5$ mm). The errors in the measurement are similar to the graph above but are not drawn for clarity. (c) Drag as a function of intruder size r_i at various speeds along with a quadratic fit in the case of each velocity ($r_h = 0.5$ mm).

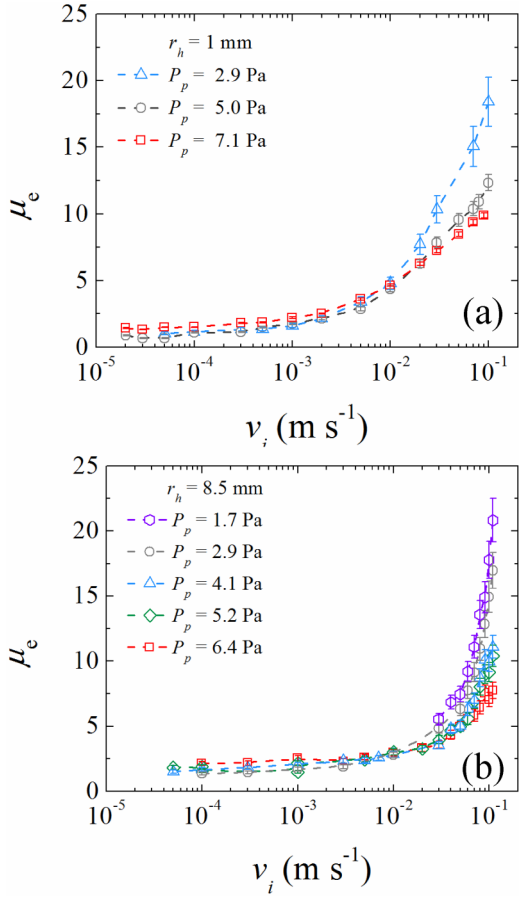

FIG. 3. Effective friction μ_e given by the ratio of the drag and the gravitational force due to the weight of the grains acting on the intruder versus v_i for various P_p in the case of (a) $r_h = 0.5$ mm and (b) $r_h = 8.5$ mm grains. In both cases μ_e is observed to increase less rapidly with increasing P_p.

similar density as the interstitial fluid, they have a profound effect on the drag experienced by the intruder.

To further investigate and illustrate the dependence of drag on system parameters, we plot the measured drag experienced by the intruder as a function of v_i in Fig. 3(b) for P_p obtained at three different depths in the case of the smaller grains. One observes that the drag increases systematically with the overburden pressure, not only at low speeds where the granular hydrogels can be expected to be in frictional contact, but also at higher speeds where the interactions between the intruder and hydrogels can be expected to be collisional. We also plot the drag experienced by the intruder as a function of its radius r_i in Fig. 3(c) for a few different v_i. From the quadratic fit to F_d corresponding to each set of v_i, we observe that the drag increases essentially with the cross-sectional area of the intruder, i.e., $F_d \propto r_i^2$. However, it should be noted that this scaling can be expected to hold provided the intruder size is larger than the grain size, with a more tortuous motion expected as the intruder size decreases below the grain size.

IV. EFFECTIVE FRICTION

To understand the observed variation of drag with system parameters, we define an effective friction μ_e experienced by the intruder as the ratio of the drag to the normal forces acting on the intruder. Estimating the normal force acting on the intruder as the overburden pressure times its cross-sectional area, we have

$$\mu_e = \frac{F_d}{P_p \pi r_i^2}. \tag{1}$$

With this definition, it can be noted that μ_e is independent of the intruder size because F_d is proportional to r_i^2, as seen from Fig. 2(c).

Focusing now on the depth dependence, μ_e as a function of v_i is plotted in Fig. 3(a) for various P_p in the case of $r_h = 0.5$ mm and in Fig. 3(b) in the case of $r_h = 8.5$ mm. We observe that μ_e corresponding to the different P_p appear to collapse at low v_i in the quasistatic regime, but clearly do not overlap for $v_i > 10^{-1}$ m s^{-1} even considering the errors in the measurements. Above this value, it appears that μ_e is effectively lower at greater depths for the same speeds. Thus, we conclude that the effective friction grows relatively less quickly with depth above the quasistatic regime as the grains are increasingly imparted momentum by the intruder.

A. Inertial and viscous numbers

We next examine the relative time scales in the system to understand the observed variation with speed and depth. These include the time scale imposed on the grains due to the motion of the intruder, the time scale over which grains rearrange due to applied pressure, and the sedimentation time scale. By comparing these time scales, we can determine the relative importance of these variables, which are affected by v_i and P_i on the observed drag.

We first consider the inertial number I corresponding to the ratio of the time scale for grains to rearrange due to the pressure and the time scale over which grains move past each other due to the shear resulting from the intruder motion. This dimensionless number is used to understand the significance of dynamic features in granular systems [13,14] and is given by $I = \dot{\gamma} d/\sqrt{P/\rho}$ in the case of grains with size d and density ρ, which are sheared uniformly with shear rate $\dot{\gamma}$ under pressure P. Because the intruder system is unsteady even when the intruder moves at constant velocity—the medium is accelerated as it moves around the intruder—a steady-state shear rate cannot be defined in our system. Nonetheless, we assume that the time scale relevant to the motion of the hydrogel grains is set by the velocity of the intruder and is thus inversely proportional to the shear rate $\dot{\gamma} = v_i/r_h$. Further, assuming the pressure $P \sim P_p$ and the grain density [25] $\rho \sim \rho_h$, we have the time scale relevant to rearrange grains to be $\sqrt{P_p/\rho_h}/r_h$. Thus,

$$I = \frac{v_i}{\sqrt{P_p/\rho_h}}. \tag{2}$$

Figure 4(a) shows I plotted as a function of v_i for various P_p. We observe that I varies over many orders of magnitude as v_i and P_p are varied in our experiments from below 10^{-3} associated with the quasistatic regime to above 10^0 associated with the collisional regime. Further, I obtained in the case of both hydrogel sizes fall on the same line that scales with v_i.

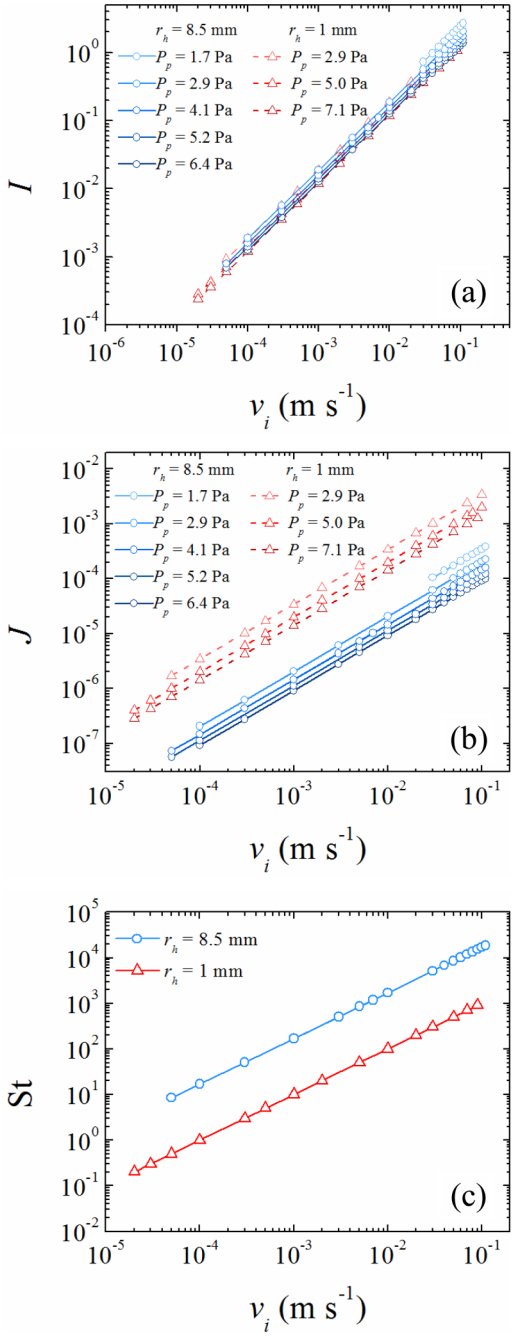

FIG. 4. (a) Inertial number I and (b) viscous number J versus v_i for various P_p probed in the study. (c) Stokes number $\mathrm{St} = I^2/J$ versus v_i for both grain sizes are observed to increase over several orders of magnitude in both cases over the range of experimental parameters investigated.

We then consider the viscous number J, which captures the relative importance of the time scales due to sedimentation of grains and shear [16]. This dimensionless number is given by $J = \eta_s \dot{\gamma} d/P$, where η_s is the viscosity of the liquid. As in the case of the inertial number, J was introduced for uniform shear rates. Assuming $\dot{\gamma} d \sim v_i$ as in the estimate of I, we obtain

$$J = \frac{\eta_s v_i}{2 P_p r_h}. \tag{3}$$

The viscous number J versus v_s is plotted in Fig. 4(b) with $\eta_s = \eta$ corresponding to the viscosity of water at 24 °C. We observe that J also varies over a wide range as a function of v_i and P_p investigated in the experiments, but is significantly smaller in magnitude compared to I. Further, J for the larger hydrogels are approximately a magnitude smaller than in the case of smaller hydrogels, because the sedimentation rate for larger particles is higher than for the smaller particles with the same density.

To further understand the relative importance of the inertial time scale and the sedimentation time scale, we examine the Stokes number St, which is given by [17] $\mathrm{St} = I^2/J$. Substituting in Eqs. (2) and (3), we have

$$\mathrm{St} = \frac{\rho_h v_i}{\eta_s}. \tag{4}$$

Plotting St in Fig. 4, we observe that it varies between 10 and 2×10^4 in the case of the larger hydrogels and between 0.2 and 10^3 in the case of the smaller hydrogels. Thus, the drag encountered appears to be in the inertial regime except in the case of the lowest velocities probed for the smaller grains. Accordingly, the inertial number appears to be the appropriate nondimensional number to describe the rate dependence of the friction as probed by the intruder velocity.

B. Rate dependence of effective friction

We plot the effective friction μ_e versus I in Figs. 5(a) and 5(b) for the small and large sized grains, respectively, investigated in our experiments. In contrast with the plots of μ_e versus v_i in Fig. 3, we find that μ_e for the various P_p clearly collapse onto a single curve for each grain size. Thus, one concludes that the stress acting on the intruder due to drag scales linearly with the pressure. A similar conclusion was reached [20] based on numerical simulations of dry granular materials investigating the role of pressure on the contact stiffness and its impact on the effective friction encountered in a granular medium. There, a deviation from linearity was found only at high pressures correlated with changes in the volume fraction of the medium. Because no significant volume fraction changes were noted in our experimental system over the range of overburden pressures encountered, the observed collapse of μ_e with P_p in Fig. 4 is consistent with that study. Further, one can note that μ_e is essentially constant over the range $10^{-4} \leqslant I \leqslant 10^{-2}$, consistent with the range typically associated with a quasistatic flow regime in granular media [26]. We further tested if the collapse improves by plotting μ_e versus K using γ as a variable [17]. No marked improvement is observed beyond what is shown in Fig. 5.

To understand the observed form of μ_e with I above the quasistatic regime, we examine the scaling for μ_e above the effective friction coefficient in the quasistatic regime μ_0 with the form

$$\mu_e(I) = \mu_0 + \alpha I^{\beta}, \tag{5}$$

where α and β are fitting constants. The value of β in particular can provide insight into the nature of the medium as probed by the intruder. Noting that μ_e is proportional to the stress at a given depth and I is proportional to the shear rate, this form is similar to the Hershel-Bulkley model for stress and strain rate

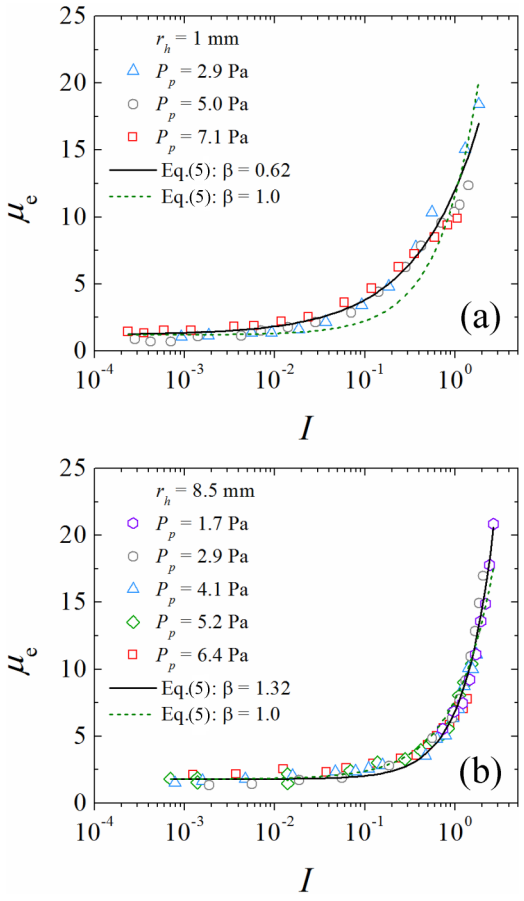

FIG. 5. (a) The effective friction μ_e corresponding to various P_p is observed to collapse onto a single curve ($r_h = 0.5$ cm and $r_i = 2.5$ cm). The fits to Eq. (5) are shown, where the solid line corresponds to $\mu_0 = 1.2$, $\alpha = 10.82 \pm 0.11$, and $\beta = 0.62 \pm 0.02$ and the dashed line to $\mu_0 = 1.2$, $\alpha = 10.38 \pm 0.35$, and $\beta = 1.0$. (b) The effective friction μ_e corresponding to various P_p is observed to observed to collapse onto a single curve ($r_h = 8.5$ mm and $r_i = 2.5$ cm). The fits to Eq. (5) are shown, where the solid line corresponds to $\mu_0 = 1.8$, $\alpha = 5.01 \pm 0.11$, and $\beta = 1.32 \pm 0.04$ and the dashed line to $\mu_0 = 1.8$, $\alpha = 5.92 \pm 0.09$, and $\beta = 1.0$.

scaling [11,12,15]. In that model, β is called the consistency index with $\beta < 1$ corresponding to a shear-thinning fluid and $\beta > 1$ corresponding to a shear thickening fluid. In the case where $\beta = 1$, the Hershel-Bulkley model reduces to the Bingham plastic model of a viscoplastic material in which the medium behaves like a viscous fluid above yield with viscosity proportional to α. Further, in the limit where grains in the medium exchange momentum during rapid collisions, one may expect Bagnold inertial granular rheology in which shear stress is proportional to the square of the strain rate [27], in which case $\beta = 2$.

We fit the functional form in Eq. (5) to the data corresponding to $r_h = 0.5$ mm in Fig. 5(a) and $r_h = 8.5$ mm in Fig. 5(b). Equation (5) is observed to capture the trend well, with $\mu_0 = 1.2, \alpha = 10.82 \pm 0.11$, and $\beta = 0.62 \pm 0.02$ in the case of the small grains and $\mu_0 = 1.8$, $\alpha = 5.01 \pm 0.11$, and $\beta = 1.32 \pm 0.04$ in the case of the large grains. We observe that μ_0 is of order 1, which implies that the force required to move the intruder is similar in magnitude to the weight of the granular sediments that have to be lifted out of the way, around the intruder.

We also fit the data by fixing $\beta = 1$ in Eq. (5) and display the result in Fig. 5 to test if the simpler Bingham model can describe the observed $\mu_e(I)$. Systematic deviations can be observed as captured by the greater dispersion in the fitting parameters that are listed in the figure caption. Thus, we conclude that the drag experienced by the intruder found at a given depth and speed can be used to predict the drag that the intruder will experience at a different set of depths and speeds using the function given in Eq. (5).

We further test if the fit of μ_e with the empirical functional form proposed by Jop *et al.* [26] for steady-state flows can describe the data $\mu_e(I) = \mu_0 + (\mu_1 - \mu_0)/(I_0/I + 1)$, where μ_1 and I_0 are constants that depend on the medium. Such a function implies that μ_e increases from μ_0 as I/I_0 increases toward 1 and then increases toward μ_1 as I/I_0 becomes well above 1. While this form also appears to give a good description of the data, we find that fitting constants do not converge with μ_1 and I_0 diverging with the increasing number of iterations used in the fitting.

Now comparing the relative values of effective friction, it can be noted that μ_e is lower at low speeds in the case of the smaller granular hydrogels compared with the larger hydrogels due to its lower volume fraction, which leads to fewer contacts between grains [28]. However, as the speed of the intruder is increased, the effective friction is observed to rise at a lower I in the case of the smaller grains. This leads μ_e to be *higher* in the case of the smaller grains than the large grains for intermediate values up to $I \sim 1$. This appears to occur because of the relative greater importance of the fluid in the case of the smaller hydrogels as captured by the lower Stokes number. Further investigations are required to fully understand these variations that depend on the nature of the medium.

V. CONCLUSION

We have measured the drag experienced by an intruder that is pulled through a sedimented granular medium immersed in water. We found that the drag experienced depends on the size of the intruder, the intruder depth in the medium, and the intruder speed. Introducing an effective friction coefficient that corresponds to the average stress experienced by the drag and normalized by the overburden pressure, we found that the friction encountered by the intruder can be parametrized by using the inertial number, which increases with the intruder velocity and as the inverse square root of the overburden pressure.

We proposed an empirical formula for the observed variation of friction with the inertial number inspired by the Hershel-Bulkley model, which depends only on the properties of the medium. Using this friction law, it was possible to relate the drag experienced by a given spherical intruder at a given depth in the medium to an intruder at a different depth in the same medium. We also related the drag encountered by an intruder of a given size to that of a different size given the observation that drag increases quadratically with the intruder size. We have further shown that the properties of the

medium, including the granular packing and fluid, can impact the empirical constants in the formula. However, further work needs to be done to fully understand these empirical constants and the detailed contribution of each parameter of the medium to the friction encountered by the intruder.

Among the broader implications of our findings is that the inertial number can be used to describe the friction encountered by an intruder in a transient flow. The effective friction in the case of granular systems has previously been only clearly shown to depend on the inertial number under steady-state conditions. This understanding of the drag experienced by an intruder in an unsteady flow not only can lead to a better description of the dynamics of passive objects in sedimented granular medium, but also has implications for a better description of active motion of organisms through sand and clay using the observed rheology.

ACKNOWLEDGMENTS

We thank Nuzhat Tani for help in performing measurements, Shomeek Mukhopadhyay and Benjamin Allen for stimulating discussions, and Abhinendra Singh for comments on the manuscript. Acknowledgment is made of the Donors of the American Chemical Society Petroleum Research Fund for partial support of this research. This work was also supported by the National Science Foundation Grant No. CBET 1335928.

[1] N. J. Balmforth, I. A. Frigaard, and G. Ovarlez, Yielding to stress: Recent developments in viscoplastic fluid mechanics, Annu. Rev. Fluid Mech. **46**, 121 (2014).

[2] M. B. Stone, R. Barry, D. P. Bernstein, M. D. Pelc, Y. K. Tsui, and P. Schiffer, Local jamming via penetration of a granular medium, Phys. Rev. E **70**, 041301 (2004).

[3] N. Gravish, P. B. Umbanhowar, and D. I. Goldman, Force and flow at the onset of drag in plowed granular media, Phys. Rev. E **89**, 042202 (2014).

[4] A. Seguin, Y. Bertho, P. Gondret, and J. Crassous, Dense Granular Flow Around a Penetrating Object: Experiment and Hydrodynamic Model, Phys. Rev. Lett. **107**, 048001 (2011).

[5] H. Katsuragi and D. J. Durian, Drag force scaling for penetration into granular media, Phys. Rev. E **87**, 052208 (2013).

[6] F. Guillard, Y. Forterre, and O. Pouliquen, Origin of a Depth-Independent Drag Force Induced by Stirring in Granular Media, Phys. Rev. Lett. **110**, 138303 (2013).

[7] D. J. Costantino, J. Bartell, K. Scheidler, and P. Schiffer, Low-velocity granular drag in reduced gravity, Phys. Rev. E **83**, 011305 (2011).

[8] S. Siavoshi, A. V. Orpe, and A. Kudrolli, Friction of a slider on a granular layer: Nonmonotonic thickness dependence and effect of boundary conditions, Phys. Rev. E **73**, 010301 (2006).

[9] B. Liu, M. Shelley, and J. Zhang, Focused Force Transmission Through an Aqueous Suspension of Granules, Phys. Rev. Lett. **105**, 188301 (2010).

[10] P. Coussot, Rheophysics of pastes: A review of microscopic modeling approaches, Soft Matter **3**, 528 (2007).

[11] W. H. Herschel and R. Bulkley, Konsistenzmessungen von gummi-benzollösungen, Kolloid Z. **39**, 291 (1926).

[12] S. Mueller, E. W. Llewellin, and H. M. Mader, The rheology of suspensions of solid particles, Proc. R. Soc. A **466**, 1201 (2010).

[13] F. Da Cruz, S. Emam, M. Prochnow, J.-N. Roux, and F. Chevoir, Rheophysics of dense granular materials: Discrete simulation of plane shear flows, Phys. Rev. E **72**, 021309 (2005).

[14] GDR MiDi, On dense granular flows, Eur. Phys. J. E **14**, 341 (2004).

[15] T. Hatano, Power-law friction in closely packed granular materials, Phys. Rev. E **75**, 060301 (2007).

[16] F. Boyer, É. Guazzelli, and O. Pouliquen, Unifying Suspension and Granular Rheology, Phys. Rev. Lett. **107**, 188301 (2011).

[17] M. Trulsson, B. Andreotti, and P. Claudin, Transition from the Viscous to Inertial Regime in Dense Suspensions, Phys. Rev. Lett. **109**, 118305 (2012).

[18] A. Panaitescu, K. Anki Reddy, and A. Kudrolli, Nucleation and Crystal Growth in Sheared Granular Sphere Packings, Phys. Rev. Lett. **108**, 108001 (2012).

[19] N. Brodu, J. A. Dijksman, and R. P. Behringer, Spanning the scales of granular materials through microscopic force imaging, Nat. Commun. **6**, 6361 (2015).

[20] A. Singh, V. Magnanimo, K. Saitoh, and S. Luding, The role of gravity or pressure and contact stiffness in granular rheology, New J. Phys. **17**, 043028 (2015).

[21] See Supplemental Material at http://link.aps.org/supplemental/10.1103/PhysRevE.95.032901 for a movie of the medium obtained using a laser sheet as the intruder advances through the medium.

[22] R. Albert, M. A. Pfeifer, A.-L. Barabasi, and P. Schiffer, Slow Drag in a Granular Medium, Phys. Rev. Lett. **82**, 205 (1999).

[23] P. Brunn, The behavior of a sphere in non-homogeneous flows of a viscoelastic fluid, Rheol. Acta **15**, 589 (1976).

[24] A. Haider and O. Levenspiel, Drag coefficient and terminal velocity of spherical and nonspherical particles, Powder Technol. **58**, 63 (1989).

[25] C. E. Brennen, A review of added mass and fluid inertial forces, Department of the Navy Report No. CR 82.010, 1982, http://resolver.caltech.edu/CaltechAUTHORS:BREncel82.

[26] P. Jop, Y. Forterre, and O. Pouliquen, A constitutive law for dense granular flows, Nature (London) **441**, 727 (2006).

[27] R. A. Bagnold, Experiments on a gravity free dispersion of large solid spheres in a Newtonian fluid under shear, Proc. R. Soc. London Ser. A **225**, 49 (1954).

[28] C. Song, P. Wang, and H. A. Makse, A phase diagram for jammed granular matter, Nature (London) **453**, 629 (2008).